AIAA-91-1604-CP

Accelerated Convergence to Steady State by Gradual Far-Field Damping

Smadar Karni *

A91-40776

The University of Michigan
Department of Mathematics
Ann Arbor, MI 48109-1003

April, 1991

Abstract

Reflections from artificial boundaries inhibit convergence of transient solutions to their steady limit. Far-field damping operators to suppress such reflections are presented for general first order hyperbolic systems, and particular reference is made to the compressible Euler equations. The damping operator has the following properties: (a) No reflections are generated due to the introduction of the damping terms and (b) Different wave systems may be damped at different rates. Feature (a) enables the attenuation of waves over relatively short length scales, while feature (b) enables the damping operator to act selectively on the outgoing waves alone, leaving the incoming waves unharmed. This property is desirable in genuine time-dependent problems where consistent information should be allowed to propagate from the artificial boundaries. Results for compressible Euler flows past aerofoils show the potential of far-field damping in substantially accelerating, particularly in fully subsonic problems.

Introduction

One important factor that influences rapid convergence of computed transient solutions to steady-state is the unsteadiness shed by the various boundary procedures. In particular, external flow calculations raise the problem of modelling open boundaries across which the fluid flows and which should ideally allow the outgoing disturbances to pass through without generating reflections. Apart from degrading time accuracy of transient solutions, reflected waves carry energies which bounce back and forth between artificial and solid boundaries dissipating very slowly[6,15] and inhibiting convergence to the steady limit.

For evolutionary problems of hyperbolic character, perfectly non-reflecting boundary conditions (BCs) exist only in one space dimension[1-3]. In multidimensional problems, perfectly absorbing BCs do not exist[3-5]. Instead, one aims at minimizing the amount of reflected energy at the boundary, often by matching the BCs to a known (asymptotic) behaviour of the solution in the far-field[1-10], or by applying heuristic boundary procedures guided by practical experience[11,12].

In this paper, we pursue a less conventional approach to suppress far-field reflections, based on modifying the governing equations in a narrow absorbing 'sponge' layer near the far-field boundary. The far-field modification is motivated by the natural decay of multidimensional disturbances which tend to zero strength as they approach infinity, and takes the form of a far-field damping operator.

Variations on the theme of far-field damping were proposed before by various authors[16-18] and applied to the solutions of external problems in various application areas. One universal feature of far-field damping is that the introduction of the damping terms creates interfaces which may generate reflections when crossed by travelling waves. Damping operators that give rise to reflections are of limited potential. In particular, in order to reduce the effect of partial, the damping operator has to be applied very gradually, smeared over a large region which may occupy up to a third of the overall domain and inaccuracies in the converged solution are to be expected. In [13,14] we show that damping operators based on a modified second order scalar wave-like equations[16-18] will inevitably give rise to partial reflections. In aerodynamis, this bears on potential flow descriptions (Full potential, Transonic Small Perturbations (TSP) etc.).

The damping operator proposed in this paper is based on a modified first order system of equations which possesses additional degrees of freedom and enables the construction of a damping operator with the following prop-

*Assistant Professor

erties:

1. travelling waves may be attenuated at an exponential rate.
2. the passage of waves accross the interface is reflection free, even under an abrupt change of coefficients.
3. different wave systems may be damped at different rates.
4. the operator depends continuously on a set of damping functions, when all set to zero the unmodified equations (and solutions) are recovered.

By property (1), the damping operator has a similar effect to moving the outer boundary to a very large distance, without incurring the penalty of large domains of computation. The question which BCs to apply at the boundary itself is of much lesser importance since wave amplitudes near the boundary are very close to zero strength. Property (2) is imperative for successful, reflection free attenuation process and for obtaining converged steady state solutions which can be trusted. Property (3) enables the design of an operator that acts only on the outgoing part of the soluion, leaving the incoming part unharmed. This feature is particularly desirable in genuinely time-dependent problems where time dependence enters through the far-field BCs and where consistent incoming information should be allowed to propagate into the domain. Property (4) makes the damping operator easy to implement. In aerodynamics, this is applicable to the Euler and Navier-Stokes flow models, as well as to the TSP equations written as a first order system.

Analysis

The Equations

The one dimensional Euler equations for inviscid non heat-conducting compressible flows in conservation form are

$$\mathbf{W}_t + \mathbf{F}(\mathbf{W})_x = 0 \tag{1}$$

$$\mathbf{W} = \begin{pmatrix} \rho \\ \rho u \\ E \end{pmatrix} \quad \mathbf{F}(\mathbf{W}) = \begin{pmatrix} \rho u \\ \rho u^2 + p \\ \rho u H \end{pmatrix}$$

where ρ, u, p and E are the density, velocity pressure and total energy respectively and $H = (E+p)/\rho$ is the specific enthalpy. We use a to denote the speed of sound and γ the specific heat ratio. Then by the perfect gas assumption, p is calculated from

$$p = (\gamma - 1)\left(E - \frac{1}{2}\rho u^2\right) \tag{2}$$

We use $\mathbf{A} = \partial\mathbf{F}/\partial\mathbf{W}$ to denote the Jacobian matrix and use $\mathbf{R} = (\mathbf{r}_1, \mathbf{r}_2, \mathbf{r}_3)$ and $\mathbf{\Lambda} = diag(\lambda_1, \lambda_2, \lambda_3)$ to denote the matrices with the eigenvectors $\mathbf{r}_k$ and eigenvalues λ_k of $\mathbf{A}$ respectively. The equations in matrix form are

$$\mathbf{W}_t + \mathbf{A}(\mathbf{W})\mathbf{W}_x = 0 \tag{3}$$

$\mathbf{A}$ is given by

$$\mathbf{A} = \begin{pmatrix} 0 & 1 & 0 \\ \frac{\gamma-3}{2}u^2 & (3-\gamma)u & \gamma - 1 \\ -u\left(H - \frac{(\gamma-1)}{2}u^2\right) & H - (\gamma-1)u^2 & \gamma u \end{pmatrix}$$

and $\mathbf{R}$ and $\mathbf{\Lambda}$ are given by

$$\begin{aligned} \mathbf{R} &= \begin{pmatrix} 1 & 1 & 1 \\ u-a & u & u+a \\ h-ua & \frac{1}{2}u^2 & H+ua \end{pmatrix} \\ \mathbf{\Lambda} &= \begin{pmatrix} u-a & 0 & 0 \\ 0 & u & 0 \\ 0 & 0 & u+a \end{pmatrix} \end{aligned} \tag{4}$$

Simple wave solutions to (1) are eigenvectors $\mathbf{r}_k$, moving at the corresponding speeds λ_k,

$$\mathbf{W}(x,t) = e^{i\omega(t-x/\lambda_k)}\mathbf{r}_k$$

General single frequency solution to (1) are superposition of simple waves

$$\mathbf{W}(x,t) = \sum_{k=1}^{3} \alpha_k e^{i\omega(t-x/\lambda_k)}\mathbf{r}_k \tag{5}$$

for some wave strengths α_k .

Far-Field Damping in 1D

In the far-field we introduce the damping operator $\mathbf{D}(\mathbf{W})$,

$$\mathbf{W}_t + \mathbf{A}(\mathbf{W})\mathbf{W}_x + \mathbf{D}(\mathbf{W})(\mathbf{W} - \mathbf{W}_\infty) = 0 \tag{6}$$

where $\mathbf{D}(\mathbf{W})$ is the 3x3 matrix

$$\begin{aligned} \mathbf{D}(\mathbf{W}) &= \mathbf{R}(\mathbf{W})\mathbf{\Delta}(\mathbf{W})\mathbf{R}^{-1}(\mathbf{W}) \\ \mathbf{\Delta}(\mathbf{W}) &= diag(d_k\lambda_k) \end{aligned} \tag{7}$$

with $\mathbf{R}(\mathbf{W})$ and λ_k the eigenvectors and eigenvalues of $\mathbf{A}$ given by (4) and d_k are arbitrary damping coefficients. General single frequency solutions to (6) are

$$\mathbf{W}(x,t) = \sum_{k=1}^{3} \alpha_k e^{-d_k x} e^{i\omega(t-x/\lambda_k)}\mathbf{r}_k \tag{8}$$

representing plane wave solutions $\mathbf{r}_k$, moving at speeds λ_k and exponentially attenuated at rates d_k. The choice

$d_k = 0$ recovers the undamped solution for the k^{th} wave. Setting all d_k to zero recovers the unmodified solution (5).

An attractive form of the damping operator which does not involve expensive matrix products can be obtained by decomposing the far-field perturbation $\mathbf{W} - \mathbf{W}_\infty$ into eigenmodes

$$\mathbf{W} - \mathbf{W}_\infty = \sum_{k=1}^{3} \alpha_k \mathbf{r}_k$$

Then,

$$\mathbf{D}(\mathbf{W})(\mathbf{W} - \mathbf{W}_\infty) = \sum_{k=1}^{3} \alpha_k \lambda_k d_k \mathbf{r}_k \qquad (9)$$

where d_k are the damping coefficients. The α_k are given by the usual expressions of the Roe's solver[19]

$$\alpha_1 = \frac{\Delta p - \rho a \Delta u}{2a^2}$$
$$\alpha_2 = \frac{\Delta \rho - a^2 \Delta p}{a^2}$$
$$\alpha_3 = \frac{\Delta p + \rho a \Delta u}{2a^2}$$

where $\Delta(\ ) = (\ ) - (\ )_\infty$ is the local perturbation of the respective flow variables about their free stream values.

Reflection Analysis

The introduction of the damping terms in the governing equations creates an interface to either side of which different equations are being solved and across which wave motion is to remain continuos. To analyze reflection and transmission properties of the damping operator, we consider the problem

$$\mathbf{W}_t + \mathbf{A}(\mathbf{W})\mathbf{W}_x + \mathbf{D}_1(\mathbf{W})(\mathbf{W} - \mathbf{W}_\infty) = 0 \quad x < 0$$
$$\mathbf{W}_t + \mathbf{A}(\mathbf{W})\mathbf{W}_x + \mathbf{D}_2(\mathbf{W})(\mathbf{W} - \mathbf{W}_\infty) = 0 \quad x > 0$$
$$[\mathbf{W}]_{x=0} = 0$$

where $[\mathbf{W}]$ denotes the jump in $\mathbf{W}$ across the interface. $\mathbf{D}_1$ and $\mathbf{D}_2$ are possibly different damping matrices of the general form

$$\begin{aligned} \mathbf{D}_1(\mathbf{W}) &= \mathbf{R}(\mathbf{W})\mathbf{\Delta}_1(\mathbf{W})\mathbf{R}^{-1}(\mathbf{W}) \\ \mathbf{D}_2(\mathbf{W}) &= \mathbf{R}(\mathbf{W})\mathbf{\Delta}_1(\mathbf{W})\mathbf{R}^{-1}(\mathbf{W}) \\ \mathbf{\Delta}_1(\mathbf{W}) &= diag(d_k^- \lambda_k) \\ \mathbf{\Delta}_2(\mathbf{W}) &= diag(d_k^+ \lambda_k) \end{aligned}$$

$d_k^\pm$ are arbitrary damping coefficients to either side of the interface $x = 0$. By (8), respective solutions take the form

$$\mathbf{W}(x,t) = \sum_{k=1}^{3} \alpha_k^- e^{-d_k^- x} e^{i\omega(t - x/\lambda_k)} \qquad x < 0$$
$$\mathbf{W}(x,t) = \sum_{k=1}^{3} \alpha_k^+ e^{-d_k^+ x} e^{i\omega(t - x/\lambda_k)} \qquad x > 0$$

Continuity across the interface reduces to

$$\mathbf{W}(0,t) = \sum_{k=1}^{3} \alpha_k^-(t)\mathbf{r}_k(\mathbf{W}) = \sum_{k=1}^{3} \alpha_k^+(t)\mathbf{r}_k(\mathbf{W}) \qquad (10)$$

The eigenvectors $\mathbf{r}_k$ are independent hence form a basis with respect to which the representation of $\mathbf{W}(0,t)$ is unique. It then follows that $\alpha_k^\pm$ satisfy

$$\alpha_k^-(t) = \alpha_k^+(t) \quad \forall t$$

implying full transmission of all waves at all times t. We summarize the main properties of the far-field damping operator:

1. analytic solution is fully transmitted across the interface for arbitrarily strong damping coefficients.
2. different wave systems may be attenuated at different rates, and in particular the outgoing waves may be damped while the incoming waves are left unharmed.

In both these respects the present damping operator is superiour to the ones in [16-18]. The latter are all based on a modified second order scalar wave-like equation, while the present operator is based on a modified first order system. A simple count of degrees of freedom confirms that if the second order wave equation is modified, there are only two free coefficients to determine the decay rates of all the wave systems, while if the same equation is transformed into the derivative space and written as a 2×2 first order system, there are four matrix elements to determine the decay rates. The additional freedom is also reflected by the fact that every second-order scalar equation can be written as a first order system, but not every first order system can be reduced to a second order scalar. It can also be verified that preservation of the eigenvectors which is imperative for full transmission of waves is not possible with a damped second order scalar [13,14].

Discrete far-field damping

Analytically, waves may be 'wiped-out' by a sudden change of damping parameters without, generating reflections. On the discrete level, the interface created due to the introduction of the damping terms is no longer a single point. It transforms into an interface 'zone', the width of which depends on that of the numerical stencil, that is on the order of accuracy of the numerical scheme. Since high order schemes possess additional spurious solution modes, the damping operator has to be applied gradually in space to ensure that the damping procedure is numerically stabe. The analytic non-reflective properties of the damping operator allows the width of the absorbing layer to be kept to a minimum, typically no more than 4-6 grid points accross the modified region.

Far-field damping and other accelerating devices

Because of its generality, the damping operator can easily be used in conjunction with other convergence accelerating devices such as multistage time integration, multiple grids and preconditioning. Note, however, that if the system is preconditioned, the damping term should be preconditioned in the same way in order to retain its non-reflective features. Note also that in multiple grid algorithms, the amount of extra computational burden incurred by the coarse and intermediate grid levels is negligible since the modified region is very narrow.

Far-Field Damping in 2D

The 2 dimensional Euler equations in conservation form are

$$\mathbf{W}_t + \mathbf{F}(\mathbf{W})_x + \mathbf{G}(\mathbf{W})_y = \mathbf{0} \tag{11}$$

with

$$\mathbf{W} = \begin{pmatrix} \rho \\ \rho u \\ \rho v \\ E \end{pmatrix} \quad \mathbf{F} = \begin{pmatrix} \rho u \\ \rho u^2 + p \\ \rho uv \\ \rho uH \end{pmatrix} \quad \mathbf{G} = \begin{pmatrix} \rho v \\ \rho uv \\ \rho u^2 + p \\ \rho vH \end{pmatrix}$$

In matrix form the equations are

$$\mathbf{W}_t + \mathbf{A}(\mathbf{W})\mathbf{W}_x + \mathbf{B}(\mathbf{W})\mathbf{W}_y = \mathbf{0} \tag{12}$$

where $\mathbf{A}$ and $\mathbf{B}$ are the Jacobian matrices $\mathbf{A} = \partial\mathbf{F}/\partial\mathbf{W}$, $\mathbf{B} = \partial\mathbf{G}/\partial\mathbf{W}$ and are given by

$$\mathbf{A} = \begin{pmatrix} 0 & 1 & 0 & 0 \\ \frac{\gamma-1}{2}q^2 - u^2 & (3-\gamma)u & -(\gamma-1)v & \gamma-1 \\ -uv & v & u & 0 \\ -u\left(H - \frac{(\gamma-1)}{2}q^2\right) & H-(\gamma-1)u^2 & -(\gamma-1)uv & \gamma u \end{pmatrix}$$

$$\mathbf{B} = \begin{pmatrix} 0 & 0 & 1 & 0 \\ -uv & v & u & 0 \\ \frac{\gamma-1}{2}q^2 - v^2 & -(\gamma-1)u & (3-\gamma)v & \gamma-1 \\ -v\left(H - \frac{(\gamma-1)}{2}q^2\right) & -(\gamma-1)uv & H-(\gamma-1)v^2 & \gamma v \end{pmatrix}$$

where $|q| = \sqrt{u^2+v^2}$ is the flow velocity. Plane wave solutions in an arbitrary direction θ satisfy

$$\mathbf{W}_t + \mathbf{M}(\theta)\mathbf{W}_{x'} = \mathbf{0} \tag{13}$$

where $x' = x\cos\theta + y\sin\theta$ and $\mathbf{M}(\theta) = \mathbf{A}(\mathbf{W})\cos\theta + \mathbf{B}(\mathbf{W})\sin\theta$. The right eigenvector matrix of $\mathbf{M}(\theta)$ is

$$\mathbf{R}(\theta) = \begin{pmatrix} 1 & 1 & 0 & 1 \\ q_n - a & q_n & 0 & q_n + a \\ q_t & q_t & 1 & q_t \\ h - q_n a & \frac{1}{2}q^2 & q_t & H + q_n a \end{pmatrix}$$

with $q_n = u\cos\theta + v\sin\theta$ and $q_t = -u\sin\theta + v\cos\theta$ the velocity components parallel and normal to the direction θ. By previous analysis we construct a θ dependent damping operator

$$\mathbf{W}_t + \mathbf{F}(\mathbf{W})_x + \mathbf{G}(\mathbf{W})_y + \mathbf{D}(\theta)(\mathbf{W} - \mathbf{W}_\infty) = 0 \tag{14}$$

with

$$\mathbf{D}(\theta) = \mathbf{R}(\theta)\mathbf{\Delta}(\theta)\mathbf{R}^{-1}(\theta)$$
$$\mathbf{\Delta}(\theta) = diag(d_k\lambda_k(\theta))$$

The choice (14) preserves the eigenvectors in an arbitrary direction θ, and has plane wave solutions,

$$\mathbf{W}(x,t) = \sum_k \alpha_k e^{-d_k x'} e^{i\omega(t-x'/\lambda_k)}\mathbf{r}_k(\theta)$$

describing plane waves moving at an arbitrary direction x' and decaying at exponential rates d_k. If all wave systems are damped at the same rate $d_k \equiv d$ for all k, equation (14) reduces to

$$\mathbf{W}_t + \mathbf{F}(\mathbf{W})_x + \mathbf{G}(\mathbf{W})_y + d\mathbf{M}(\theta)(\mathbf{W} - \mathbf{W}_\infty) = 0$$

It is, however, not necessary to constrain all wave systems by the same decay rate and the damping operator may remain in its general form (14). Here again a more attractive form of the damping operator is

$$\mathbf{D}(\theta)(\mathbf{W} - \mathbf{W}_\infty) = \sum_k \alpha_k\lambda_k d_k \mathbf{r}_k(\theta) \tag{15}$$

with α_k the Roe's wave strengths.

Damping strategies

The direction θ in which waves are damped varies from one grid point to the next and its choice is problem dependent. Here various damping strategies may be adopted. One possibility is to damp the waves in the direction normal to the outer boundary. In this case, $\theta = \theta_{i,j}$ is calculated *once* at the beginning of the computation. Another possibilty is to choose $\theta_{i,j}$ in the direction of the outgoing waves. This direction may be extracted from local gradients of the flow variables and needs to be computed at every time step. A possible recipe for choosing θ for flow past an aerofoil geometry is illustrated in Figure (1). The expected effect of damping on far-field solution is to 'push' the solution towards the free stream values. Indeed, when damping is applied, flow variables close to the outer boundary have converged values which are very close to the free stream values. Movies of residual convergence history show that outgoing waves do not penetrate more than very few cells into the 'sponge' layer before they are damped[15]. A typical effect of far-field damping on the converged Mach number distribution on the aerofoil surface is illustrated in Figure (2).

Far-field damping and Enthalpy damping

Enthalpy damping, originally proposed by Jameson, Schmidt and Turkel[10], proved a very successful device for accelerating convergence of unsteady compressible inviscid flows to their steady limit. It was derived by reducing the unsteady Euler equations to the wave equation, modifying the wave equation by adding a damping term to obtain decaying solutions as $t \rightarrow \infty$, and transforming the modified equation back to the Euler equations. The result is a set of modified equations

$$\mathbf{W}_t + \mathbf{F}(\mathbf{W})_x + \mathbf{G}(\mathbf{W})_y + d(\mathbf{H} - \mathbf{H}_\infty)\tilde{\mathbf{W}} = 0 \qquad (16)$$

with $\mathbf{H}_\infty$ the free stream enthalpy. Since the steady state enthalpy is constant along streamlines, if all streamlines originate from a uniform free stream, steady solutions of (16) are also steady solutions of (11). The coefficient d is then chosen to optimize convergence rate. Enthalpy damping was later analyzed by Jespersen[20] who made the following observations: When $d = 0$, (16) form a hyperbolic system, and possess frozen coefficient solutions of the form

$$\mathbf{W}(x,t) = e^{-i\xi x'} \sum_k \alpha_k e^{\omega_k t} \mathbf{r}_k(\theta)$$

with $\omega_k = \omega_k(\xi)$ purely imaginary. He also showed that under certain conditions, taking $d > 0$ pulls ω_k off the imaginary axis into the left half of the complex plane, yielding exponential time decay of solutions and consequently accelerated convergence. In fact, what he showed was that out of the four eigenvalues $\omega_k(\xi)$, only three are pulled off while one always remains on the imaginary axis. Hence, even with enthalpy damping, not all solutions decay in time. That Euler solutions do converge to a steady limit he accredited to the numerical dissipation introduced by the stable time integration procedure.

It is easy to verify that the present damping operator pulls *all* eigenvalues off the imaginary axis. Moreover, they can be pulled as far off the imaginary axis as one wishes, by choosing appropriate values for the damping coefficients d_k. Enthalpy damped solutions are not time accurate, but they converge to the correct steady limit. By contrast, the present modified system (14) does not possess same steady solutions as the original system (11). On the contrary, one expects far-field solutions to decay faster towards their $(\,)_\infty$ values. On the other hand, since the damping terms are non-reflective, at least in a one-dimensional asymptotic sense, their introduction in (14) should not destroy time accuracy in the inner unmodified region and is expected to converge to the same steady limit over that region (see Figure (2)).

Numerical Results

Numerical algorithm and boundary conditions

The method of solution is Hall's variation[11] of the cell vertex scheme with LW time integration, originally proposed by Ni[12]. The time increment at cell vertex 1 (see Figure (3)) is given by,

$$\begin{aligned}
\delta\mathbf{W}_1 &= \Delta_1\mathbf{W} + \Delta_2\mathbf{W} \\
\Delta_1\mathbf{W} &= \frac{S_A\Delta\mathbf{W}_A + S_B\Delta\mathbf{W}_B + S_C\Delta\mathbf{W}_C + S_D\Delta\mathbf{W}_D}{S_A + S_B + S_C + S_D} \\
\Delta_2\mathbf{W} &= \frac{\Delta t}{4S_1}\times \\
&\quad ((\Delta\mathbf{F}_C - \Delta\mathbf{F}_A)(y_B - y_D) + (\Delta\mathbf{F}_D - \Delta\mathbf{F}_B)(y_C - y_A) + \\
&\quad (\Delta\mathbf{G}_A - \Delta\mathbf{G}_C)(x_B - x_D) + (\Delta\mathbf{G}_B - \Delta\mathbf{G}_D)(x_C - x_A))
\end{aligned}$$

with S_A denoting the area of cell A, Δt denoting the time step and changes at cell centers are given by

$$\begin{aligned}
\Delta\mathbf{W}_C &= \frac{\Delta t}{2S_C}\times \\
&\quad ((\mathbf{F}_3 - \mathbf{F}_1)(y_2 - y_4) + (\mathbf{F}_4 - \mathbf{F}_2)(y_3 - y_1) + \\
&\quad (\mathbf{G}_1 - \mathbf{G}_3)(x_2 - x_4) + (\mathbf{G}_2 - \mathbf{G}_4)(x_3 - x_1))
\end{aligned}$$

$$\begin{aligned}
\Delta\mathbf{F}_C = \left(\frac{\partial F}{\partial W}\right)_C \Delta W_C &= \frac{1}{4}(A_1 + A_2 + A_3 + A_4)\,\Delta W_C \\
\Delta\mathbf{G}_C = \left(\frac{\partial G}{\partial W}\right)_C \Delta W_C &= \frac{1}{4}(B_1 + B_2 + B_3 + B_4)\,\Delta W_C
\end{aligned}$$

with A_1 and B_1 denoting the Jacobian matrices at cell vertices. The scheme also uses artificial smoothing to suppres spatial oscillations, the details of which can be found in [11].

Boundary conditions: The original scheme proposed by Hall is designed for the calculation of steady solutions. The energy equation is omitted and pressure is calculated from Bernoulli's equation, using free stream enthalpy. The boundary recipes recommended by Hall are as following: At inflow, tangential velocity and entropy are specified, normal velocity is extrapolated using a one-sided version of the interior scheme. At outflow, free stream pressure is specified and velocity components are extrapolated using one-sided version of the interior scheme. These boundary recipes were selected by Hall after extensive experiments with various boundary recipes, including non-reflective boundary conditions. They have proved better suited for the calculation of steady solutions, in that they yielded faster convergence than the non-reflective BCs. On the solid wall, the interior scheme is applied and a simple tangency condition is applied to the predicted solution. In

the tests presented in this paper, Hall's method is applied to the full 4×4 system (11). Hall's boundary recipes are augmented by specifying the free stream enthaply at inflow and extrapolating enthalpy at outflow, using the same one-sided version of the interior scheme. It is the expereince of the author that, like in the reduced system case, these boundary recipes yield faster convergence than non-reflecting boundary conditions, and that the spatial decay of converged flow field variables towards the free stream values is monotone.

Damping term: The non-homogeneous system (14) is solved by an operator split algorithm where in the first stage the solution $\mathbf{W}$ gets updated by the flux terms and in the second stage, a pointwise time integrator is used to account for the effects of the damping operator. Since accuracy is not required in the modified layer in the far-field, a first order Euler time integrator is used.

Numerical tests

Steady solutions are calculated for transonic and subsonic flows past a symmetric non-lifting circular aerofoil of 10% height/chord length ratio. The unsteady equations (14) are integrated and convergence is declared when nodal changes of all conserved quantities are less than 10^{-6}. We use an aligned mesh with 32 evenly spaced cells on the aerofoil and linearly stretching cells on either of its sides and in the vertical direction (see Figure (4)). Converged steady state drag and normal force coefficients are obtained using

$$C_D = \sum_k \frac{(p_i - p_\infty)\Delta y_i}{\rho_\infty u_\infty^2}$$

$$C_N = \sum_k \frac{(p_i - p_\infty)\Delta x_i}{\rho_\infty u_\infty^2}$$

Owing to symmetry, the solution is calculated only on the top half of the aerofoil, with reflective BCs applied along the line of symmetry. Consequently, the normal force coefficient C_N does not vanish and serves to assess the effect of the far-field boundary and the far-field damping on the accuracy of the converged solution. To minimize the effect of the far-field BCs on the converged solution, we conducted a series of experiments with the outer boundary placed at various distances, until the converged solution ceases to change (changes in C_N and $C_D \leq 10^{-4}$). The results of transonic and subsonic flow calculations are summarized in Table (1). For the tests conducted, it was found that boundary distance of $\sim$ 10 chord lengths is sufficient and solutions of tests (5) and (11) are considered 'accurate'. The respective converged Mach number and pressure profiles are shown in Figure (5). The effect of far-field damping on the convergence characteristics of the solution is summarized in Tables (2) and (3). In the Tables, Boundary Thickness indicates the number of nodes accross the modified region and Direction of Modification indicates the direction in which waves are damped (X for inflow and outflow boundaries, Y for top boundary and X-Y for both). The first line in each table serves as a bench mark and indicates a computation with the BCs described in the previous section. Tests (2) through (7) use the same BCs together with far-field damping. In Test (8), all outer boundaries are crudely overspecified to free stream conditions, and far-field damping is applied. Test (8) is particularly relevant to the ocurrence of a characteristic boundary, since the type of a characteristic boundary changes almost at random during the transient phase as a result of small numerical errors. A conventional boundary treatment that depends on the boundary type will also be random and may end up shedding unsteadiness and delaying convergence.

Transonic Test Case

Results are summarized in Table (2). In all cases far-field damping accelerates convergence to steady states and is found relatively insensitive to parameters like Boundary Thickness and Attenuation rate. Comparison of Tests (1) and (6) reveals a handsome 35% drop in the number of iterations to steady state, while relative differences in C_N and C_D are less than 1%. Absolute differences in both are of order 10^{-4}. Convergence histories of Tests (1) and (6) are compared in Figure (6). One stiking result is that even the overspecified case (8) converges almost as rapidly as (6). This indicates that in all previous cases, most energy is absorbed by the damping operator and not by the BCs.

Subsonic Test Case

Results are sumarized in Table (3). Here, the impact of far-field damping is even more dramatic, yielding an impressive drop of over 60% in number of iterations to steady state, with relative changes in C_N and C_D well under 0.5% (compare Tests (1) and (3)). The more pronounced impact of the damping is to be expected, since in the transonic case, convergence is delayed by the formation of the shock wave as well. The rapid convergence of Test (8) should also be noted, demonstrating the effectiveness of energy absorption by the damping operator even when the boundary is overspecified. Convergence histories of Tests (1) and (3) show that the periodic nature of convergence, attributable to far-field reflections[15], is almost entirely removed (see figure (7)).

Summary

A framework has been given for the construction of damping operators to suppress reflections from artificial boundaries for general first order hyperbolic systems. Particular reference is made to the compressible Euler equations. The damping operator selectively damps the outgoing part of the solution over short length scales, without affecting the incoming part of the solution and without

generating reflections. Two dimensional steady Euler calculations of subsonic and transonic flows past symmetric aerofoils demonstrate substantial improvement in convergence characteristics, with a particularly sharp impact in the fully subsonic case. The results also indicate that far-field damping is an attractive alternative to conventional boundary treatments near characteristic boundaries where boundary type changes almost at random due to small numerical errors, and where customizing the boundary procedures to a random boundary type may end up shedding unsteadiness.

Acknowledgements

I thank P.L. Roe for inspiring this work and for being a constant source of advice throughout its course. I thank A.D. French for providing the basic code for the Euler calculations.

References

[1] Orlanski I., (1976), "A simple boundary condition for unbounded hyperbolic problems", *J Comp Phys*, **21**, 251-269.
[2] Hedstrom G.W., (1979), " Non-reflecting boundary conditions for nonlinear hyperbolic systems", *J Comp Phys*, **30**, 222-237.
[3] Engquist B. and Majda A., (1977), "Absorbing boundary conditions for the numerical simulation of waves" *Maths of Comp*, **31**, 629-651.
[4] Bayliss A. and Turkel E., (1980), "Radiation boundary conditions for wave-like equations", *Comm Pure Appl Math*, **33**, 707-725.
[5] Giles M., (1989), "Non-Reflecting boundary conditions for Euler equation calculations", *AIAA* 89-1942-CP.
[6] Rudy H. and Strikwerda J.C., (1980), "A non-reflecting outflow boundary condition for subsonic Navier Stokes calculations", *J Comp Phys*, **36**, 55-70.
[7] Hagstrom T. and Hariharan S.I., (1988), "Accurate boundary conditions for exterior problems in gas dynamics", *Math of Comm*, **51**, 581-597.
[8] Lindman E.L., (1975), " 'Free-space' boundary conditions for the time dependent wave equation", *J Comp Phys*, **18**, 66-78.
[9] Higdon R.L., (1986), "Absorbing boundary conditions for difference approximations to the multidimentional wave equation", *Math of Comp*, **47**, 437-459.
[10] Jameson A., Schmidt W. and Turkel E., (1981), "Numerical solution of the Euler equations by finite volume methods using Runge-Kutta time stepping schemes", *AIAA* 81-1259.
[11] Hall M.G., (1985), "Cell vertex multigrid schemes for solutions of the Euler equations", in K.W. Morton and M.J. Baines (eds.) *Numerical Methods for Fluid Dynamics II*, Oxford University Press, 303-345.
[12] Ni R-H., (1981), "A multiple grid scheme for solving the Euler equations", *AIAA* 81-1025.
[13] Karni S., (1990), "Far-field boundaries and their numerical treatment", PhD Thesis, Cranfield Institute of Technology.
[14] Karni S., (1991), "Far-field filtering operators for the suppression of wave reflections from artificial boundaries", (in preparation).
[15] Mazaheri K. and Roe P.L., (1991), "New light on numerical boundary conditions", AIAA 10th Computational Fluid Dynamics Conference, Honolulu, Hawaii.
[16] Kosloff R. and Kosloff D., (1986), "Absorbing boundaries for wave propagation problems", *J comp Phys*, **63**, 363-374.
[17] Hanson M. and Petschek J., (1976), "A boundary condition for significantly reducing boundary reflections with a Lagrangien mesh", *J Comp Phys*, **21**, 333-339.
[18] Israeli M. and Orszag S.A., (1981), "Approximation of radiation boundary conditions", *J Comp Phys*, **41**, 115-135.
[19] Roe P.L., (1981), "Approximate Riemann solver, Parameter vectors, and difference schemes", *J Comp Phys*, **43**, 357-372.
[20] Jespersen D.C., (1985), "Enthalpy damping for the steady Euler equations", *Appl Num Math*, **1**, 417-432.

Test No.	*Boundary Distance*	*Grid Size*	C_N	C_D	*No. of Iterations*
	$\mathbf{M_\infty = 0.5}$				
1	1.00000	65×17	$-.281787$	0.001360	5390
2	2.64355	85×27	$-.313781$	0.000478	5168
3	4.70732	97×33	$-.317904$	0.000363	6358
4	6.90649	105×37	$-.318964$	0.000353	6503
5	10.12629	113×41	$-.319406$	0.000358	6418
6	12.25938	117×43	$-.319529$	0.000342	6289
	$\mathbf{M_\infty = 0.75}$				
7	1.00000	65×17	$-.355310$	0.005332	1637
8	2.64355	85×27	$-.437400$	0.012209	3919
9	4.70732	97×33	$-.450744$	0.013626	4540
10	6.90649	105×37	$-.460982$	0.014580	5342
11	10.12629	113×41	$-.462811$	0.014788	5528
12	12.25938	117×43	$-.463335$	0.014851	5879

Table I – Converged values of C_N and C_D vs boundary distance

Test No.	*Damping Coefs*	*Boundary Thickness*	*Direction of Mod.*	*Number of Iterations*	C_N	C_D
1	0.0	0	–	5528	$-.46281$	.01479
2	0.5	6	X	5368	$-.46443$	.01515
3	0.5	6	Y	4799	$-.46116$	.01462
4	0.4	5	Y	4926	$-.46158$	.01466
5	0.6	5	Y	4884	$-.46144$	.01465
6	0.5	6	$X-Y$	3621	$-.46355$	.01510
7	0.4	6	$X-Y$	3646	$-.46355$	.01510
8	0.5	6	$X-Y$	3712	$-.46372$	.01510

Table II – Parameter study of far – field damping – Transonic case

Test No.	*Damping coefs*	*Boundary thickness*	*Direction of Mod*	*Number of Iterations*	C_N	C_D
1	0.0	0	–	6418	$-.31941$	.00036
2	0.5	6	X	5573	$-.31976$	.00036
3	0.5	6	$X-Y$	2404	$-.32007$	.00036
4	0.4	6	$X-Y$	2418	$-.32005$	.00036
5	0.5	6	Y	3192	$-.31985$	.00036
6	0.4	5	Y	3383	$-.31995$	.00036
7	0.5	5	Y	3352	$-.31997$	.00037
8	0.5	5	$X-Y$	2401	$-.32001$	.00036

Table III – Parameter study of far – field damping – Subsonic case

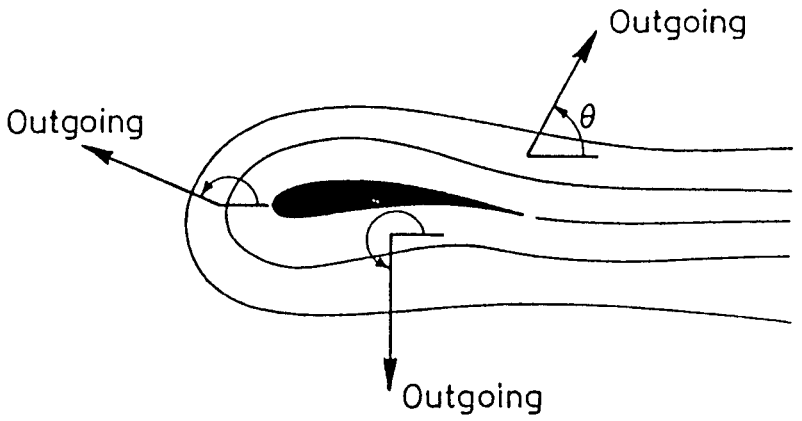

Figure 1: A possible recipe for choosing θ for flow calculation past aerofoils.

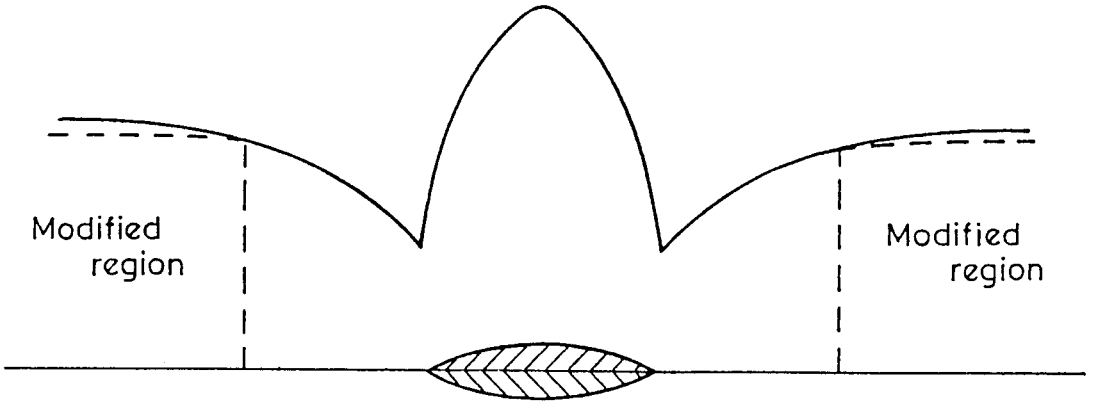

Figure 2: A typical effect of far-field damping on the converged subsonic Mach number profiles: Undamped (dashed) and damped (solid) solutions.

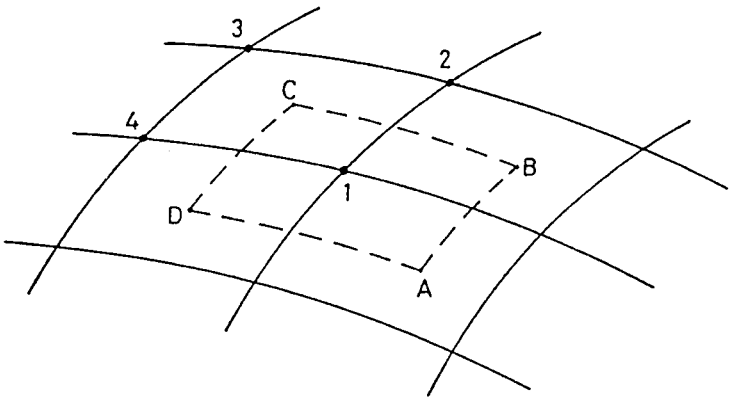

Figure 3: Grid notation for Hall's numerical algorithm.

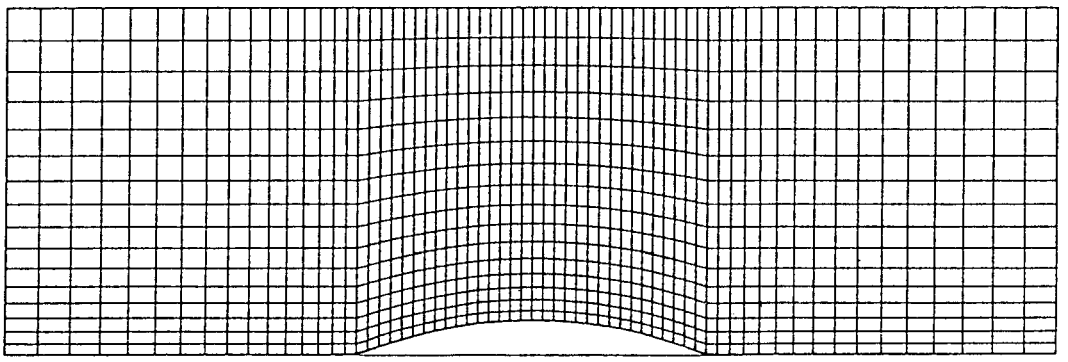

Figure 4: Numerical grid for non-lifting aerofoil calculation.

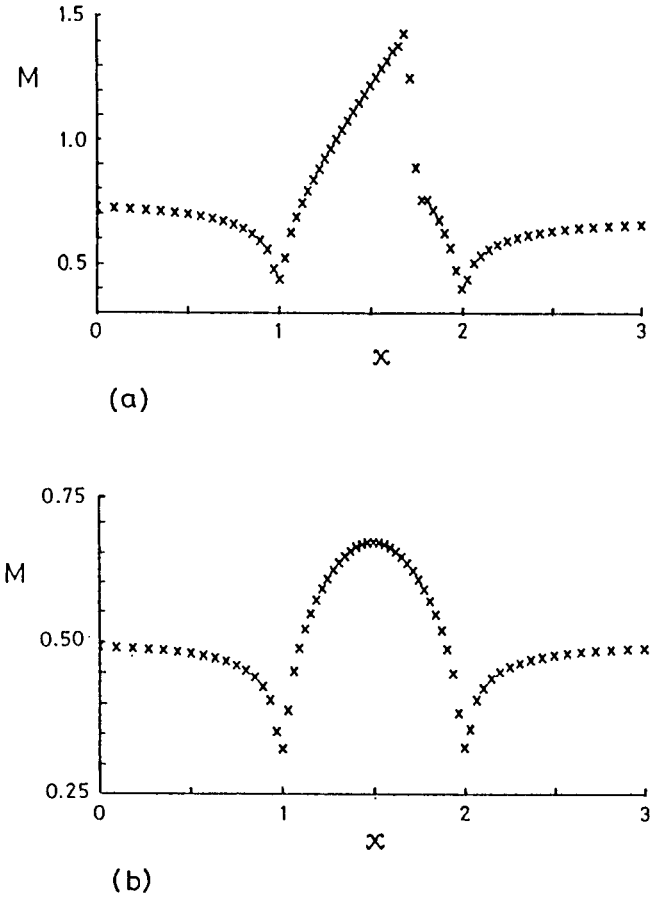

Figure 5: Converged Mach number profiles for Tests (5) and (11) in Table (1): (a)Transonic and (b) subsonic cases.

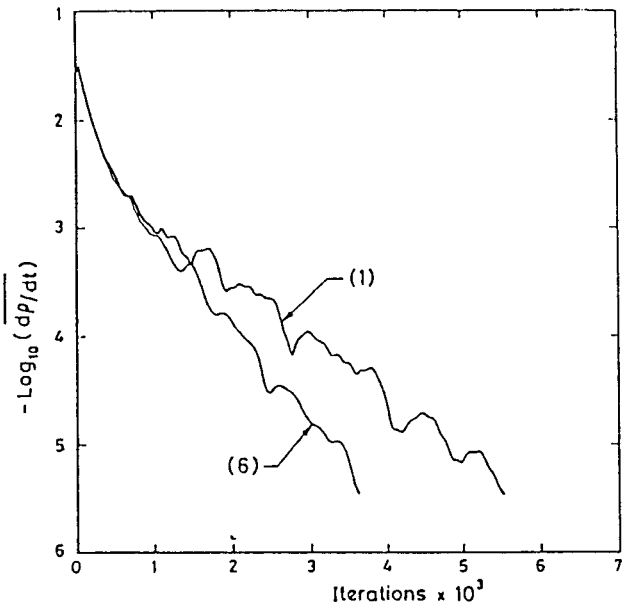

Figure 6: Convergence histories for transonic test: Average density residuals vs iteration number for Tests number (1) and (6) in Table (2).

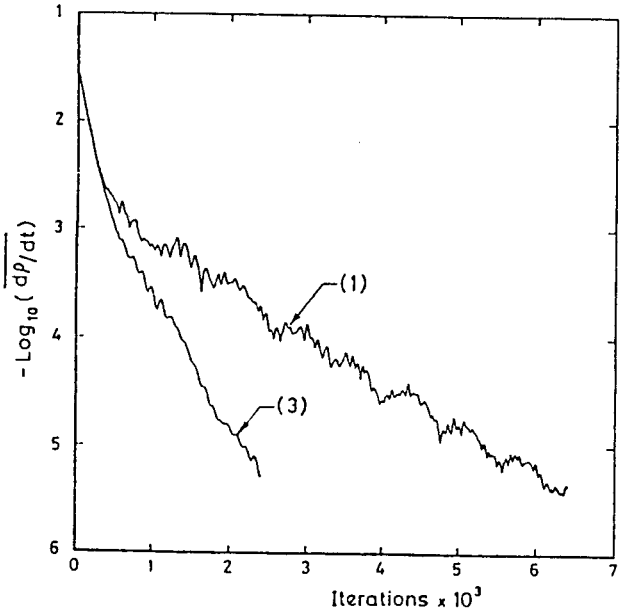

Figure 7: Convergence histories for subsonic test: Average density residuals vs iteration number for Tests number (1) and (3) in Table (3).